Accurate optical simulation of nano-particle based internal scattering layers for light outcoupling from organic light emitting diodes

Amos Egel, Guillaume Gomard, Siegfried W. Kettlitz, Uli Lemmer

Light Technology Institute and Institute of Microstructure Technology, Karlsruhe Institute of Technology, Karlsruhe, Germany

We present a numerical strategy for the accurate simulation of light extraction from organic light emitting diodes (OLEDs) comprising an internal nano-particle based scattering layer. On the one hand, the light emission and propagation through the OLED thin film system (including the scattering layer) is treated by means of rigorous wave optics calculations using the T-matrix formalism. On the other hand, the propagation through the substrate is modelled in a ray optics approach. The results from the wave optics calculations enter in terms of the initial substrate radiation pattern and the bidirectional reflectivity distribution (BRDF) of the OLED stack with scattering layer. In order to correct for the truncation error due to a finite number of particles in the simulations, we extrapolate the results to infinitely extended scattering layers. As an application example, we estimate the optimal particle filling fraction for an internal scattering layer in a realistic OLED geometry. The presented treatment is designed to emerge from electromagnetic theory with as few additional assumptions as possible. It could thus serve as a baseline to validate faster but approximate simulation approaches.

1 Introduction

In organic light emitting diodes (OLEDs), photons are generated inside a thin film system of high refractive index materials. As a consequence, light is trapped in the device due to waveguiding effects, which significantly limit the efficiency [1, 2]. Bound modes like surface plasmon polaritons (SPPs) and thin film waveguide modes are excited in the OLED layer stack. In addition, total internal reflection at the substrate / air interface leads to light trapping in the substrate, see figure 1.

A common approach to improve the device efficiency is to introduce scattering structures into the OLED stack. They break the lateral translation symmetry and couple waveguide modes with radiation modes. The present paper focuses on planarized nano-particle based scattering layers that are inserted between the substrate and the transparent electrode of a typical OLED stack - a configuration that has attracted both scientific and industrial attention [3–8] as it uniquely gathers a number of benefits. The electrically active layer system is not altered by the scattering layer that can in fact be regarded as a part of the substrate. The deposition of the host material / nano-particle composite layer can take place at room temperature in ambient environment, and no further structuring process of the outcoupling layer needs to take place, such that low cost fabrication is feasible. Finally, in contrast to ordered scattering structures, such as Bragg grating and photonic crystals, particle layers define a random geometry and therefore lead to an emission characteristics without spectral or angular distortions. In addition to the outcoupling of thin film waveguide modes, scattering particle layers diffuse the reflection at the back electrode of the OLED and thereby also improve the outcoupling from the substrate trapped light.

Accurate simulations with regard to the light extraction from OLEDs with internal scattering particle layers are extremely challenging. One reason is the broad range of the involved length scales, that reach from the particle diameters and layer thicknesses in the nanometer scale, over the decay length of the waveguide modes that is typically in the micron scale to the substrate thickness in the millimeter scale.

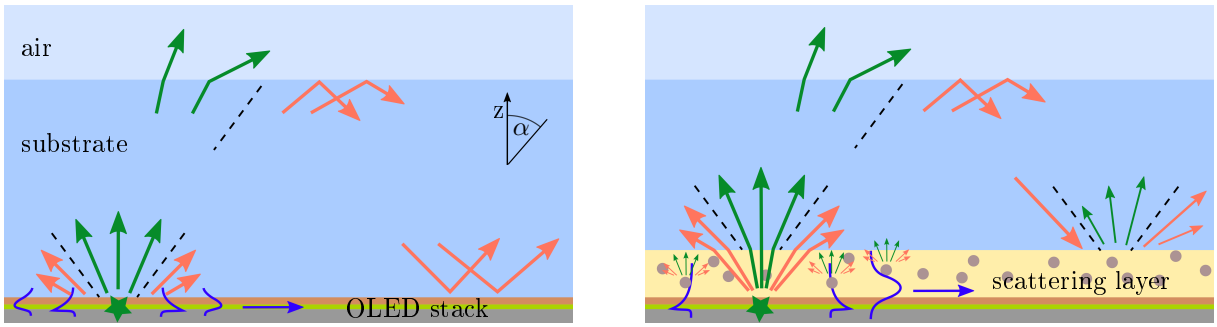

Figure 1: Left: Typical bottom-emitting OLED with substrate, transparent electrode, emitter layer, metal electrode. Green arrows represent light rays inside the so called "escape cone", i.e., with a propagation angle α smaller than the critical angle. Red arrows correspond to light that is trapped inside the substrate. The blue curves are bound modes in the thin film system. The z-axis of our coordinate system is normal to the layer interfaces. Right: OLED with scattering layer containing nano-particles. Thin-film bound photons scatter and are partly coupled into the substrate far field (small arrows). Substrate guided light rays are diffusely reflected by the OLED thin film system including scattering layer, and are partly redirected into the escape cone.

Previous studies have either assumed a microscopic approach [7, 9] or employed a ray optics model for the scattering layer [10]. In either case, certain assumptions have to be made on the microscopic or the macroscopic aspects of light propagation. In order to verify the validity of these assumptions, a comprehensive numerical approach is required which is capable of both: Correctly treating vectorial and wave effects *and* assessing the macroscopic optical device parameters. Due to the vast computational complexity, this problem has not been solved yet.

In a previous study, we have reported on an efficient and accurate computational scheme to calculate the electromagnetic fields excited by dipole emission in a layer system comprising scattering particle layers by means of the T-matrix formalism [11]. The aim of the present paper is to embed this computational scheme into a comprehensive numerical approach that allows to deliver estimates of the macroscopic outcoupling efficiency. Our main contributions are:

- To set up a ray optics framework for light propagation in the thick substrate layer (section 2.2). Wave optics calculations enter through the initial radiation pattern and the bidirectional reflectivity distribution function (BRDF) of the OLED thin film system with scattering layer.
- To propose an extrapolation scheme to correct for the error introduced by the finite number of modelled scattering particles and to examine its validity (section 2.4).
- To apply the numerical approach to an example OLED configuration and use it to estimate the optimal particle volume density in an internal scattering layer (section 3).

Finally, the paper is completed by a comparison of the proposed method to related work in section 4.

2 Methods

Consider an OLED structure with internal scattering layer, as depicted in Fig. 1 (right). In order to compute the emission of light into free space, we proceed in three steps: First, the propagation of radiation through the substrate into the air is described in a ray optics framework. This model relies on two input parameters: the initial power flux from the OLED into the substrate, and the BRDF of the OLED with scattering layer, for beams incident from the substrate side. Thus, the second and third steps are to

respectively calculate the power emitted by the OLED's active layer into the substrate and the BRDF of the OLED with scattering layer in wave optics simulations. Before describing these steps in detail, we define the extraction pattern as the central quantity of interest, and define the statement of the problem as finding an estimate for this quantity.

2.1 The extraction pattern

With regard to light outcoupling, the most important figure of merit is the *extraction efficiency*. It is defined as the radiated power divided by the total power converted into light. An extraction efficiency of 1 would correspond to an optically perfect OLED, whereas absorption and light trapping in general lead to significantly smaller numbers. The second important feature of interest is the spectral and angular *emission pattern*, i.e., the relative distribution of the outcoupled power into emission angles and wavelengths. It incorporates information about possible preferred directions or color-angle distortions in the emission.

In this paper, we restrict ourselves to the important case of systems which are statistically isotropic with respect to the azimuthal angle. Then, for a given wavelength, the emission pattern depends solely on the polar angle α. From the viewpoint of optical simulations, the extraction efficiency and the emission pattern are governed by one function, the *polar extraction pattern* X_j^{air}, which is the central figure in the following analysis. It is defined by the relation

$$X_j^{\mathrm{air}}(\lambda,\alpha) = \frac{1}{P_0(\lambda)} \frac{\mathrm{d}}{\mathrm{d}\alpha} P_j^{\mathrm{air}}(\lambda), \tag{1}$$

where $P_j^{\mathrm{air}}(\lambda)$ is the total emitted power of light with polarization j (1 for TE and 2 for TM) and wavelength λ, and $P_0(\lambda)$ denotes the internal spectrum, i.e., the rate of photons generated at a certain vacuum wavelength times the photon energy. If the extraction pattern and the internal spectrum are known, the extraction efficiency can be calculated according to

$$\eta^{\mathrm{air}} = \sum_{j=1}^{2} \frac{\int \mathrm{d}\lambda\, P_0(\lambda) \int \mathrm{d}\alpha\, X_j^{\mathrm{air}}(\lambda,\alpha)}{\int \mathrm{d}\lambda\, P_0(\lambda)}.$$

In other words, the extraction pattern defines, how many photons with a given wavelength will be outcoupled into a given direction and polarization state, divided by the total number of generated photons with that wavelength. For its calculation, we model the luminescent molecules using classical monochromatic electric point dipole sources [12]. As the light output of an OLED originates from many molecules emitting simultaneously but independently from each other, the measured emission corresponds to an incoherent average with respect to a statistical ensemble of emitting dipole orientations and positions within the active layer. As for the internal spectrum, we assume that the probability distribution of emitting dipole orientations and positions is known a priori.

A big challenge with regard to the numerical effort of optical simulations is given by the dimensions of the system. We assume in this paper that the lateral size of the OLED device is much larger than all layer thicknesses. Neglecting edge effects, the lateral dimensions can be modeled as infinite. However, due to the growing numerical effort for a large number of scattering particles, the microscopic calculations will rely on a truncation of the scattering sample size. This introduces a systematic error on the simulation results which has to be corrected for.

Thus, we can state the problem as follows: to estimate the extraction pattern, averaged over all random distributions (scattering layer characteristics and emitter characteristics), in the limit of a scattering particle layer that is infinitely extended in the lateral dimensions.

The simulation method involves both, wave optics calculations for the thin film system including the scattering layer, and ray optics calculations for the substrate layer. We start with the ray optics formalism.

2.2 Light propagation in the substrate: ray optics model

Inside the substrate, the propagation of light can be modelled by a net distribution of power over the propagation angles and polarizations. The treatment is similar to the one presented in [10]. To achieve a discrete notation for the radiation distributions, we introduce a regular grid of $N_\alpha + 1$ polar angles between 0 and $\pi/2$:

$$\alpha_i = i\frac{\pi}{2N_\alpha},\ i = 0, \ldots, N_\alpha.$$

Then, we can define the *binned forward and backward propagating radiation distributions,* $X^{\uparrow}_{j,i}$ and $X^{\downarrow}_{j,i}$, as the radiant flux of light with polarization j, propagating in the polar angle interval $[\alpha_{i-1}, \alpha_i]$ of the substrate far field in positive or negative z-direction, respectively, divided by the total electromagnetic power dissipated into the system. A priori, the distributions $X^{\uparrow}_{j,i}$ and $X^{\downarrow}_{j,i}$ are unknown. They depend on the following three figures: The *binned initial substrate pattern* $X^0_{j,i}$, the *transmittance* $T_{j,i}$ at the substrate / air interface, and finally the *binned bidirectional reflectivity* $R_{j,j',i,i'}$ at the OLED thin film stack including the scattering layer. Note that each of these figures also depends on the emission wavelength λ. However, we will omit the dependency on the wavelength from the notation for the sake of brevity.

The binned initial substrate pattern $X^0_{j,i}$ is defined in analogy to the binned radiation distributions $X^{\uparrow\downarrow}_{j,i}$: It is the expected value of the radiant flux of light with polarization j emitted into the polar angle interval $[\alpha_{i-1}, \alpha_i]$ of the substrate far field by dipole emission in the active layer of the OLED, divided by the total electromagnetic power dissipated by that dipole. The binned initial substrate pattern will be evaluated by means of wave optics calculations, confer section 2.3.2. For the case of a planar interface between substrate and air[1], the transmittance $T_{j,i} = T_j(\alpha_i)$ is just the Fresnel transmittance. The binned bidirectional reflectivity is defined by the relation

$$I^{\mathrm{R}}_{j,i} = R_{j,j',i,i'} I^{\mathrm{E}}_{j',i'},$$

where $I^{\mathrm{R}}_{j,i}$ is the radiant flux of light with polarization j reflected by the OLED thin film system including scattering layer into the polar angle interval $[\alpha_{i-1}, \alpha_i]$ of the substrate far field, as a reaction to an incoming radiant flux $I^{\mathrm{E}}_{j'i'}$ that is incident from the polar angle $\alpha_{i'}$ with polarization j'.

The key step is now to write the forward propagating radiation $X^{\uparrow}$ as the sum of the initial substrate pattern plus the reflection of the backward propagating radiation $X^{\downarrow}_{\mathrm{sub}}$:

$$X^{\uparrow}_{j,i} = X^0_{j,i} + \sum_{j',i'} R_{j,j',i,i'} X^{\downarrow}_{j',i'} \tag{2}$$

Further, the backward propagating radiation in the substrate is given by the specular reflection of the forward propagating radiation at the substrate / air interface

$$X^{\downarrow}_{j,i} = (1 - T_{j,i})\, X^{\uparrow}_{j,i}. \tag{3}$$

Substituting $X^{\downarrow}$ in (2) by the right hand side of (3) leads to

$$X^{\uparrow}_{j,i} = X^0_{j,i} + \sum_{j',i'} R_{j,j',i,i'} (1 - T_{j',i'})\, X^{\uparrow}_{j',i'}. \tag{4}$$

Equation 4 can be rewritten as

$$\sum_{j',i'} \left[1 - R_{j,j',i,i'} (1 - T_{j',i'})\right] X^{\uparrow}_{j',i'} = X^0_{j,i} \tag{5}$$

[1] In case of an OLED with additional external outcoupling structures (e.g. micro lens arrays), the scalar transmittance can be replaced by a bidirectional distribution in a straightforward manner.

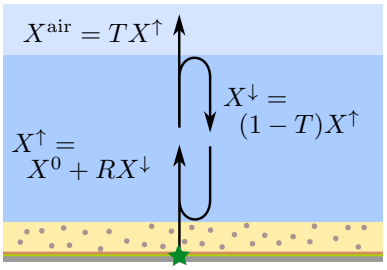

Figure 2: Forward and backward propagating radiation in the substrate.

which is a finite system of linear equations for the unknown discretized intensity distribution $X^{\uparrow}_{j,i}$. After solving (5), the *binned ambient extraction pattern* can be evaluated. We set

$$X^{\text{air}}_{j,i} = T_{j,i_{\text{sub}}} X^{\uparrow}_{j,i_{\text{sub}}} \frac{\mathrm{d}\alpha}{\mathrm{d}\alpha_i}, \tag{6}$$

where α is the polar angle in the substrate that corresponds to α_i via Snell's law:

$$\sin\alpha_i = n_{\text{sub}} \sin\alpha,$$

with the substrate's refractive index n_{sub}, such that

$$\frac{\mathrm{d}\alpha}{\mathrm{d}\alpha_i} = \frac{\cos\alpha_i}{n_{\text{sub}}\cos\alpha}.$$

The index i_{sub} in (6) refers to the interval of polar angles that contains the angle α: $\alpha \in [\alpha_{i_{\text{sub}}-1}, \alpha_{i_{\text{sub}}}]$. Finally, the continuous extraction pattern reads

$$X^{\text{air}}_{j}(\lambda, \alpha_i) = \frac{2N_\alpha}{\pi} X^{\text{air}}_{j,i}$$

which can be interpolated to arbitrary propagation angles α.

2.3 Propagation in the thin film system with scattering layer: wave optics model

The wave optics treatment aims at solving Maxwell's equations for the OLED thin film geometry including the scattering particles and a point dipole source (section 2.3.2) or an incident Gaussian wave bundle (section 2.3.3), respectively. An opaque metal cathode is modelled as a layer of semi-infinite nature, as well as the substrate layer which is modelled incoherently such that it appears as a semi-infinite layer in the wave optics calculations.

2.3.1 T-matrix formalism for N particles in a planarly layered medium

For the case of a thin film OLED geometry without scattering structures, the electrodynamic problem of a point dipole source embedded in a system of plane parallel interfaces can be solved analytically up to the evaluation of a so called Sommerfeld integral [12, 13]. But in the presence of scattering centers that break the 2D translation symmetry of the planarly layered medium, the electromagnetic fields cannot be determined in closed form anymore. Inspired by earliear work on scattering objects near a planar interface [14–19], we have recently reported on a computational scheme to rigorously model the electromagnetic field of a dipole source embedded in a planarly layered thin film system with multiple scattering particles inside [11]. A central feature of the method is the representation of the electromagnetic field in terms of both plane and spherical vector wave functions, and the transformation from one representation to the other.

In general, the main steps of the computational scheme are:

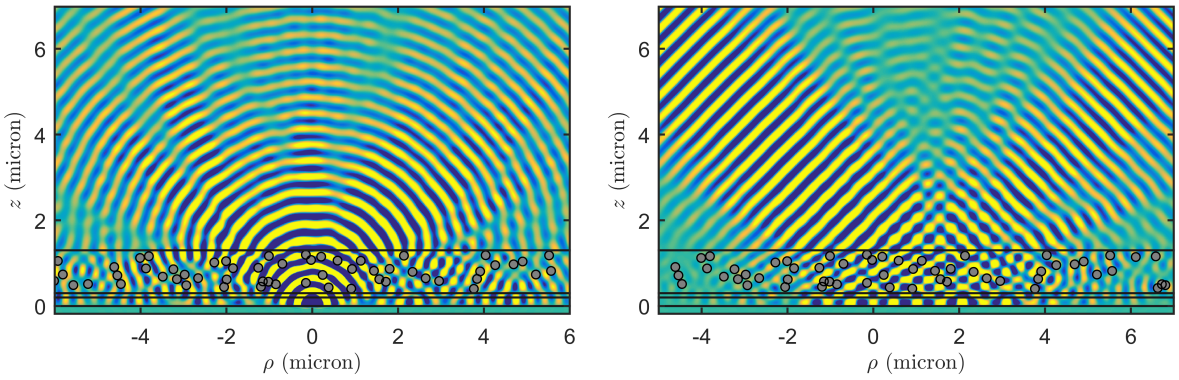

Figure 3: A cut through the simulated 3D electric field distribution in the substrate and the thin film system including scattering spheres for dipole excitation (left, dipole moment oriented out-of-plane), and for an incident Gaussian wave bundle (right). The gray circles indicate nearby spheres, and the lines show the OLED layer interfaces formed by the different functional layers: substrate (top), scattering layer, transparent electrode, emitter layer, metal electrode (bottom). Animations of the electric field propagation are attached as supplementary files to the online version of this article.

1. To expand the propagated initial field in a series of regular spherical vector wave functions (SVWFs) $\mathbf{\Psi}_n^{(1)}$ relative to each particle's center coordinate $\mathbf{r}_S$:

$$\mathbf{E}^{\mathrm{in}}(\mathbf{r}) = \sum_n a_n^{S,\mathrm{in}} \mathbf{\Psi}_n^{(1)}(\mathbf{r} - \mathbf{r}_S)$$

   The resulting expansion coefficients are called $a_n^{S,\mathrm{in}}$, where S indicates the scattering particle and n is a multi index for the SVWF polarization and multipole order. For a total number of N_S particles and a multipole truncation order at $n = n_{\max}$, the coefficient vector describing the initial field at all particles has $N_S n_{\max}$ entries. Note that the initial field can be either the field of an emissive point dipole representing a luminescent molecule or an incoming beam representing the field that has been reflected at the substrate / air interface. In the latter case, the treatment given in [11] is modified in a straightforward manner to account for an incoming wave bundle as the initial field instead of the initial dipole excitation.

2. To determine the scattering particle coupling matrices $W_{nn'}^{\mathrm{D},SS'}$ and $W_{nn'}^{\mathrm{R},SS'}$. These matrices describe how outgoing SVWFs relative to the center coordinate of particle S' will excite regular SVWFs relative to the center coordinate of particle S. The matrix W^{D} encodes the direct interaction, whereas the matrix W^{R} accounts for the layer system mediated interaction between two particles, i.e., the coupling due to reflections at layer interfaces. While the direct interaction is given by the SVWF addition theorem [15] that can be constructed from closed form expressions, the layer system mediated interaction matrix involves the numerical evaluation of a Sommerfeld integral for each matrix entry [20].

3. To compute the transition matrices (T-matrix) [21, 22] of the scattering particles. The T-matrix relates the regular SVWF coefficients a_n of the incoming field to the outgoing SVWF coefficients b_n of the scattered field for a given particle. For homogeneous spherical particles, the T-matrix is just a diagonal matrix containing the Mie coefficients. For more general particle geometries, numerical methods can be used to determine the T-matrix, e.g. the null field method with discrete sources [23].

4. To solve the linear system for the scattered field coefficients b_n^S,

$$\sum_{S',n'} M_{nn'}^{SS'} b_{n'}^{S'} = \sum_{n'} T_{nn'}^{S} a_{n'}^{S,\mathrm{in}} \tag{7}$$

with

$$M_{nn'}^{SS'} = 1 - \sum_{n''} T_{nn''}^{S} \left(W_{n''n'}^{\mathrm{D},SS'} + W_{n''n}^{\mathrm{R},SS'} \right).$$

(7) is a system of $N_S n_{\max}$ linear equations for $N_S n_{\max}$ unknowns. The system can be either solved by direct methods or iteratively. A direct solution using LU factorization has the advantage that the factorized matrix can be reused for repeated simulations with a modified initial field and therefore with modified a^{in}. For a fixed random particle configuration, the initial substrate radiation pattern as well as the whole bidirectional reflectivity distribution can then be computed with only one single matrix factorization. However, the maximal matrix dimension that can be handled by the computer system is practically limited by the memory. Consequently, only a limited number of particles for a given maximal multipole order can be accounted for. As an alternative, (7) can be solved iteratively, e.g.,by means of the bi-conjugate gradient stabilized (BiCGStab) method. Then, the coupling coefficients can be computed "on the fly", as no knowledge of the full matrix M is necessary but only matrix-vector multiplications need to be carried out. To minimize the numerical effort, the coupling coefficients are precomputed in a lookup table [20] for later interpolation. However, the drawback of using an iterative method is that the intermediate results cannot be reused for a repeated simulation with modified initial field coefficients a^{in}.

5. To evaluate the relevant power flux figures. In this post processing step, the plane wave radiation patterns in the relevant layers are calculated from the scattered field coefficient vector b. Although the numerical effort of this calculation can also be significant, it only scales linear to the number of particles. For large systems, it therefore takes much less time than step 4.

Due to its superior efficiency, the above described scheme allows for an accurate calculation of the electromagnetic fields in mesoscopic samples that span several tens of microns and that contain thousands of particles. This is currently barely possible with other purely numerical tools like finite-difference or finite-elements methods, and would require tremendous computer resources. However, for a reduced number of particles, we have performed finite-element simulations with the software package COMSOL in order to compare the electric field to our calculations. The results are shown in a supplementary file to the online version of this article and are in excellent agreement to the results acquired with the T-matrix method, which demonstrates the validity of our implementation.

2.3.2 Dipole dissipated power and initial substrate radiant intensity

The above described wave optics computation is employed with an electric point dipole source as the initial field. The total dissipated power of the dipole can be evaluated using Poynting's theorem [12,24]

$$\begin{aligned} P^{\mathrm{dip}} &= \int \mathrm{d}^3\mathbf{r}\, \mathbf{E}(\mathbf{r}) \cdot \mathbf{j}_{\mathrm{dip}}(\mathbf{r}) \\ &= \mathbf{E}(\mathbf{r}_{\mathrm{dip}}) \cdot \mathbf{d}, \end{aligned}$$

where $\mathbf{j}_{\mathrm{dip}}(\mathbf{r}) = (\mathrm{i}\omega)^{-1} \delta(\mathbf{r} - \mathbf{r}_{\mathrm{dip}})\, \mathbf{d}$ is the dipole's current density. On the other hand, the substrate radiation power is calculated from the time averaged Poynting vector for the total electromagnetic field, i.e., the dipole field plus the scattered field from all particles,

$$P^{\mathrm{sub}} = \frac{1}{2} \Re \int \mathrm{d}^2\mathbf{r}_{\parallel} \left(\mathbf{E}^*(\mathbf{r}) \times \mathbf{H}(\mathbf{r}) \right) \cdot \hat{\mathbf{e}}_z.$$

Expanding $\mathbf{E}$ and $\mathbf{H}$ in plane waves and using orthogonality, the above can be transformed into an expression of the type

$$P^{\mathrm{sub}} = \int \mathrm{d}^2\Omega \, I_j^{\mathrm{sub}}(\Omega), \tag{8}$$

where Ω is the solid angle in the substrate and $I_j^{\mathrm{sub}}(\Omega)$ is the initial substrate radiant intensity (compare equation 30 of [11]). The next step is to convert (8) into the form required by (2), by defining the binned simulated substrate pattern as

$$X_{j,i}^{0,\mathrm{sim}}(\rho) = \frac{\pi \sin\alpha_i}{2N_\alpha P^{\mathrm{dip}}} \int_0^{2\pi} \mathrm{d}\beta \, I_j^{\mathrm{sub}}(\Omega).$$

Here, the solid angle Ω corresponds to the polar angle α_i and the azimuthal angle β. Further, the parameter ρ indicates the radius of the cylindrical volume filled with scattering particles in the simulation (at a fixed volume density). The superscript "sim" refers to the fact that the above quantities belong to a single wave optics simulation. Then, the initial extraction pattern can then be estimated as

$$X_{j,i}^{0} = \left\langle \lim_{\rho\to\infty} X_{j,i}^{0,\mathrm{sim}}(\rho) \right\rangle_{\mathrm{sim}}, \tag{9}$$

where $\langle . \rangle_{\mathrm{sim}}$ denotes the average over several simulations with different random particle configurations as well as dipole orientations and positions in the emitter layer. A method for the practical evaluation of the limit towards infinite scattering layers will be presented and discussed in section 2.4.

2.3.3 Specular and Diffuse Reflection

We use a monochromatic narrow Gaussian wave bundle with vacuum wavelength λ to model the initial field of an incident light ray, such that the exciting field is localized within the lateral extent of the scattering sample, see Figure (3) (right).

$$\mathbf{E}_{\mathrm{in}}(\mathbf{r}) = \int \mathrm{d}^2\mathbf{k}_\parallel g_{\mathrm{in}}(\mathbf{k}_\parallel) \, \mathrm{e}^{\mathrm{i}(k_x x + k_y y - k_z z)} \hat{\mathbf{e}}_{j_{\mathrm{in}}}$$

with

$$g_{\mathrm{in}}(\mathbf{k}_\parallel) = \exp\left(-\frac{\left|\mathbf{k}_\parallel - \mathbf{k}_{\parallel,\mathrm{in}}\right|^2}{2\sigma_{\mathrm{in}}^2} \right).$$

Here, $\mathbf{k}_\parallel$ denotes the in-plane wavevector (k_x, k_y), whereas $k_z = \sqrt{k_{\mathrm{sub}}^2 - \mathbf{k}_\parallel^2}$ is fixed by the dispersion relation in the substrate. The polarization and the propagation direction of the incoming wave bundle are denoted by j_{in} and $\mathbf{k}_{\parallel,\mathrm{in}}$, respectively, whereas σ_{in} refers to the angular width of the wave bundle and $\hat{\mathbf{e}}_{j_{\mathrm{in}}}$ is the unit vector in azimuthal ($j_{\mathrm{in}} = 1$) or polar ($j_{\mathrm{in}} = 2$) direction. The power associated with this incoming beam is given by

$$P^{\mathrm{E}} = \pi\lambda\Re \int \mathrm{d}^2\mathbf{k}_\parallel k_z \left| g_{\mathrm{in}}(\mathbf{k}_\parallel) \right|^2,$$

where $\Re$ stands for the real part. To derive the initial field coefficients $a_n^{S,\mathrm{in}}$ for an incoming Gaussian wave bundle, the expressions given in [11] for the case of dipole excitation need to be modified in a straightforward manner. The wave optics simulations are then performed as described in section 2.3.1, yielding a 2D angle and polarization resolved reflected substrate intensity $I_j^{\mathrm{R}}(\Omega)$ with total reflected power

$$P^{\mathrm{R}} = \sum_j \int \mathrm{d}^2\Omega \, I_j^{\mathrm{R}}(\Omega).$$

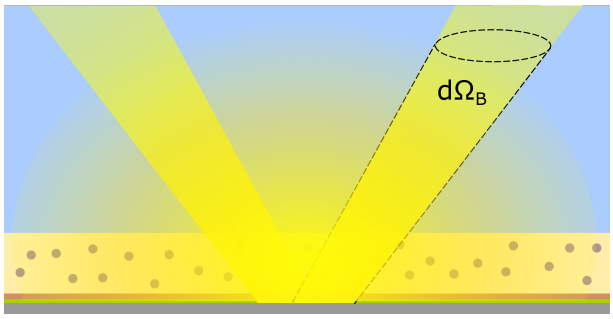

Figure 4: For an incident Gaussian wave bundle, the specular part of the reflection is collected by the solid angle interval B.

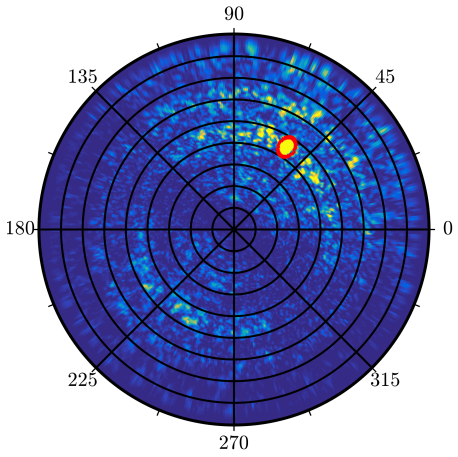

Figure 5: Simulated TE-polarized reflection $I_{\mathrm{ref},1}^{\mathrm{sim}}(\Omega_{\mathrm{sub}})$ of a TE-polarized Gaussian wave bundle with a polar angle of incidence $\alpha_{\mathrm{in}} = 45°$ and an azimuthal angle of incidence $\beta_{\mathrm{in}} = 57°$. The center of the image corresponds to radiation propagating perpendicular to the substrate / scattering layer interface. The concentric circles correspond to polar reflection angles in steps of 10°. One can see the diffuse reflection as a speckle distribution, whereas the specular reflection is visible as a bright spot with a width that corresponds to the angular width of the incoming wave bundle. The red line marks the region B attributed to the specular reflection.

The radiant intensity $I_j^{\mathrm{R}}(\Omega)$ will be the physical quantity that we use to estimate the reflectivity distribution. However, it will be necessary to first separate the specular from the diffuse part of the reflection. In general, the binned reflectance distribution reads

$$R_{j,j',i,i'} = R_{j,j',i,i'}^{\mathrm{diff},} + \delta_{jj'}\delta_{ii'}R_{j,i}^{\mathrm{spec}},$$

where R^{diff} denotes the diffuse reflection and R^{spec} corresponds to the specular reflection. If we directly use $I_j^{\mathrm{R}}(\Omega)$ to estimate the reflectivity distribution, the so obtained result will be affected by the finite width of the initial wave packet in k-space, which effects a convolution of the reflectivity distribution with the initial distribution. In fact, the simulated reflected intensity $I_j^{\mathrm{R}}(\Omega)$ shows a maximum in the specular direction, which is broadened by the angular width of the incoming beam. However, to allow for a clean separation of the diffuse and specular part of the reflectivity, the radiant flux reflected into the broadened peak needs to be attributed to the specular signal. Thus, we suggest to cut a small cone around $\mathbf{k}_{\parallel,\mathrm{in}}$ from the total reflected radiation pattern, and interpret the far field power radiated into this cone as the specular reflection, as depicted in Fig. 4. We define the cone of specular directions as

$$B = \left\{ \Omega, \left| \mathbf{k}_{\parallel} - \mathbf{k}_{\parallel,\mathrm{in}} \right|^2 \leq 9\sigma_{\mathrm{in}}^2 \right\},$$

where $\mathbf{k}_{\parallel}$ is the in-plane wave vector that belongs to the substrate solid angle Ω. Further, the cut-out reflected radiant intensity can be defined as

$$\tilde{I}_j^{\mathrm{R}}(\Omega) = \begin{cases} 0 & \text{if } \Omega \in B \text{ and } j = j_{\mathrm{in}} \\ I_j^{\mathrm{ref}}(\Omega) & \text{else.} \end{cases}$$

The specularly and diffusely reflected radiant flux then read

$$\begin{aligned} P^{\mathrm{spec}} &= \int_B \mathrm{d}^2\Omega I_{j_{\mathrm{in}}}^{\mathrm{ref}}(\Omega) \\ P^{\mathrm{diff}} &= \sum_j \int \mathrm{d}^2\Omega\, \tilde{I}_j^{\mathrm{R}}(\Omega). \end{aligned}$$

In analogy to the binned radiation distributions defined in section 2.2, we define the simulated binned diffuse reflectivity as

$$R_{j,j',i,i'}^{\mathrm{diff,sim}}(\rho) = \frac{\pi \sin \alpha_{i'}}{2N_\alpha P^{\mathrm{E}}} \int_0^{2\pi} \mathrm{d}\beta\, \tilde{I}_j^{\mathrm{R}}(\Omega)$$

for an incoming beam with polar angle $\alpha_{i'}$ and polarization j' and a scattering layer that is truncated at a radial distance ρ from the center of the incoming beam at fixed particle density. As before, the solid angle Ω belongs to the polar angle α_i and the azimuthal angle β. For the specular part, we obtain the simulated binned specular reflectivity as

$$R_{j,i}^{\mathrm{spec,sim}}(\rho) = \frac{P^{\mathrm{spec}}}{P^{\mathrm{E}}}$$

This treatment corrects the estimation of the specular reflection at the cost of another error: The power that is in fact diffusely reflected into B, i.e., a small cone around the specular direction, will be wrongly attributed to the specular reflection (see Fig. 5). However, for a narrow bundle (i.e., $\sigma_{\mathrm{in}} \ll \omega/c$) this error is negligible.

In practice, we can then use the following estimator for the bidirectional reflectivity:

$$R_{j,j',i,i'} = \left\langle \lim_{\rho\to\infty} \left(R_{j,j',i,i'}^{\mathrm{diff,sim}}(\rho) + \delta_{jj'}\delta_{ii'} R_{j,i}^{\mathrm{spec,sim}}(\rho) \right) \right\rangle_{\mathrm{sim}}.$$

As before, $\langle\cdot\rangle$ stands for an average over the random scattering particle configuration. In order to keep the simulation effort at a manageable level, a fixed number of incoming beams can be used and the reflectivity distribution can be interpolated with respect to $\alpha_{i'}$. A way to perform the limit to infinite scattering layers in praxis will be given in the next section.

2.4 Extrapolation to Infinite Scattering Layers

For a wave optics simulation with a finite number of scattering particles, the scattering sample is limited to a certain domain. Thus, the extraction of the power in thin-film guided modes is necessarily incomplete, because the outcoupling contribution from particles beyond the ensemble domain is cut off. In the following, we will discuss a method to estimate the impact of this error and extrapolate the outcoupling results to a scattering layer extended infinitely in the horizontal plane. From heuristic arguments, we will derive a model for the behavior of X^0 and R as a function of the particle domain's radius ρ. The treatment is equivalent to the one presented in [25] in the context of photonic crystal structures for light management in light emitting diodes.

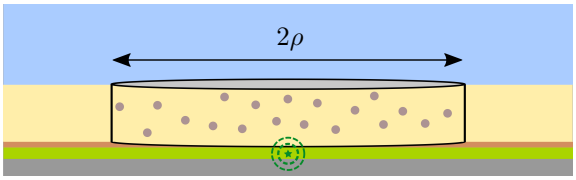

Figure 6: Approximation of an infinite scattering layer through a series of fnite scattering layers truncated in cylinders with growing radius ρ. .

Consider a cylinder, the central axis of which is perpendicular to the layer interfaces and goes through the excitation position (dipole source or incoming beam center). The cylinder is bounded in the z-direction by the scattering layer interfaces. In general, the electromagnetic power P_{sl} flowing through the side surfaces of this cylinder , will be a function of the cylinder radius ρ. For small ρ, this function $P_{\mathrm{sl}}(\rho)$ is characterized by a complicated interplay between the radiation modes and the various thin film waveguide modes excited by the dipole source or the incoming beam, and nothing can be said about its general functional dependence. But for large ρ the power guided in the individual waveguide modes reaches an equilibrium distribution, due to scattering. Then, both absorption and outcoupling into the substrate far field modes lead to a gradual extinction of the total power $P_{\mathrm{sl}}(\rho)$. For sufficiently large ρ, we write the ansatz

$$\frac{\mathrm{d}P_{\mathrm{sl}}(\rho)}{\mathrm{d}\rho} = -\gamma_{\mathrm{absorb}} P_{\mathrm{sl}}(\rho) - \gamma_{\mathrm{rad}} P_{\mathrm{sl}}(\rho) \quad \text{for } \rho \geq \rho_{\mathrm{min}}$$

where γ_{absorb} is an effective inverse absorption length and γ_{rad} is an effective inverse scattering length for the energy transfer from waveguide modes into the substrate far field. The waveguided power in the scattering layer then takes the form

$$P_{\mathrm{sl}}(\rho) = P_{\mathrm{sl}}(\rho_{\mathrm{min}}) \exp\left(-(\gamma_{\mathrm{absorb}} + \gamma_{\mathrm{rad}})(\rho - \rho_{\mathrm{min}})\right) \text{ for } \rho \geq \rho_{\mathrm{min}}.$$

Consequently, if the scattering simulations are truncated at a radius $\rho > \rho_{\mathrm{min}}$, the power coupled into the substrate is underestimated by an amount

$$\int_{\rho}^{\infty} \mathrm{d}\rho' \, \gamma_{\mathrm{rad}} P_{\mathrm{sl}}(\rho') = \tilde{P} \exp(-\gamma\rho)$$

where

$$\begin{aligned} \gamma &= \gamma_{\mathrm{absorb}} + \gamma_{\mathrm{rad}} \\ \tilde{P} &= P_{\mathrm{sl}}(\rho_{\mathrm{min}}) \, \mathrm{e}^{\gamma\rho_{\mathrm{min}}} \frac{\gamma_{\mathrm{rad}}}{\gamma}. \end{aligned}$$

The simulated power flux P^{sub} as a function of the truncation radius $\rho > \rho_{\mathrm{min}}$ is thus expected to behave like

$$P^{\mathrm{sub}}(\rho) = P_{\infty} - \tilde{P} \exp(-\gamma\rho). \tag{10}$$

The idea is now, to fit this expression to a number of simulation results for different values of the particle domain radius ρ in order to estimate the asymptotic substrate power P_{∞}. Let us first consider the case of the initial extraction pattern X^0. First, we generate a series of N_{sim} simulations for a single dipole source, with ascending number of particles that are bounded in cylindrical domains with radius $\rho_1 < \rho_2 < \ldots < \rho_{N_{\mathrm{sim}}}$. Then, we use expression (10) to extrapolate the initial substrate power resulting from these simulations to $\rho = \infty$. For the angle dependent extrapolated initial extraction pattern, we can then estimate

$$\lim_{\rho\to\infty} X^{0,\mathrm{sim}}_{j,i}(\rho) \approx \frac{\left[P^{\mathrm{sub}}\right]_{\rho\to\infty}}{\left[P^{\mathrm{sub}}\right]_{\rho_{N_{\mathrm{sim}}}}} X^{0,\mathrm{sim}}_{j,i}(\rho_{N_{\mathrm{sim}}}).$$

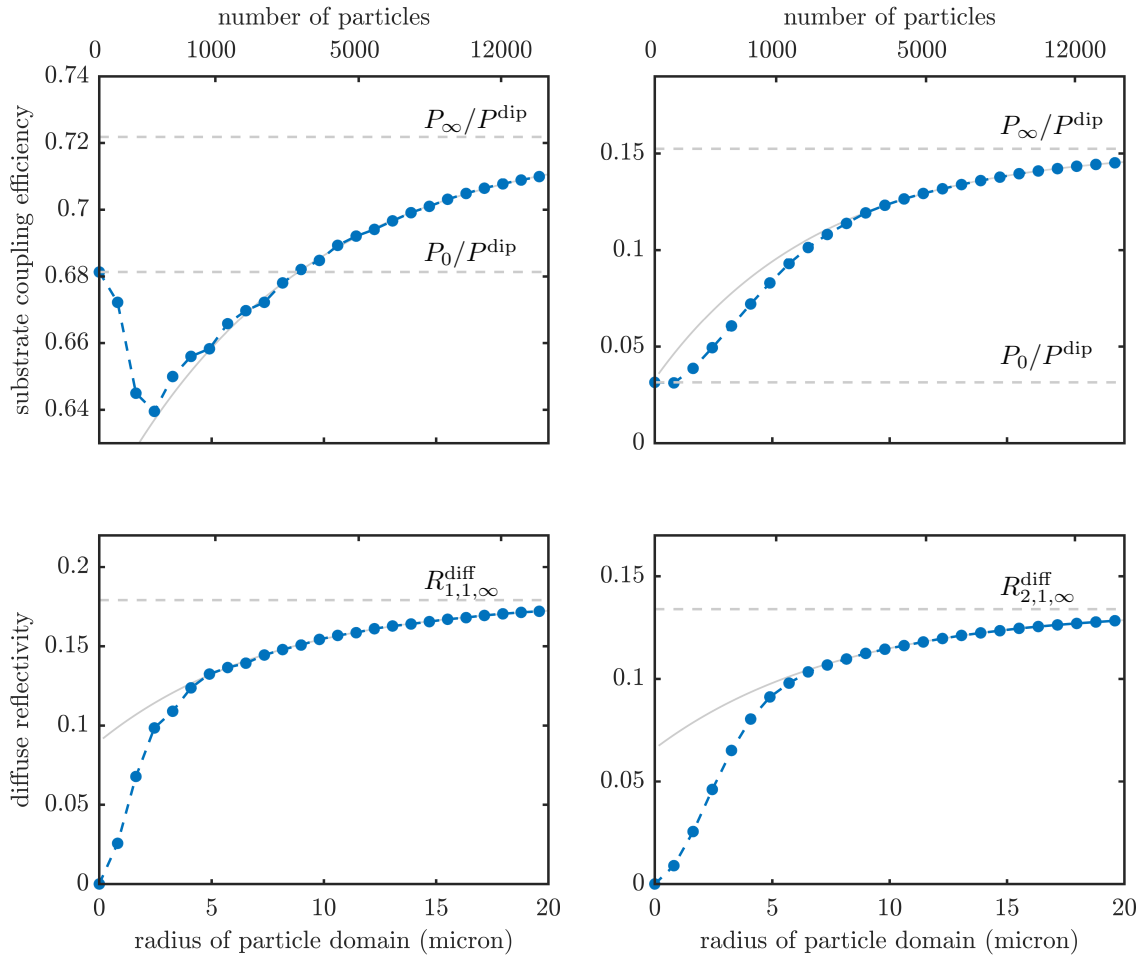

Figure 7: Simulated power emitted/reflected into the substrate as a function of the lateral dimension of the particle sample, at a constant volume density of 5 %. Top row: Substrate coupling efficiency $P^{\mathrm{sub}}/P^{\mathrm{dip}}$ for parallel (left) and perpendicular (right) dipole orientation. Bottom row: TE (left) and TM (right) polarized diffusely reflected power for an incoming TE polarized Gaussian wave bundle with an incident angle of 45°. The gray solid lines depict the best fit of expression (10).

In other words, the extrapolation is done only for the integrated power flux into the substrate, whereas the angular distribution is taken from the simulation result for the maximal number of particles, which is then scaled to the extrapolated power flux.

For the extrapolation of the bidirectional reflectivity, we proceed in the same way: For a fixed incident angle, we perform a series of simulations and split the simulated reflected intensity distribution into a diffuse and specular part, as described in section 2.3.3. Then, we use expression (10) to extrapolate the total diffusely reflected power for each polarization, and use the result to scale the 2D diffuse angular intensity distribution. For the specular part, an extrapolation is in general not necessary as the specular reflection is mainly affected by single scattering such that the simulated value is not expected to change for values of ρ that are large compared to the spatial width of the incoming beam, $\sigma_\rho = \sigma_{\mathrm{in}}^{-1}$.

$$\lim_{\rho\to\infty} R^{\mathrm{diff,sim}}_{j,j',i,i'}(\rho) = \frac{\left[P^{\mathrm{diff}}\right]_{\rho\to\infty}}{\left[P^{\mathrm{diff}}\right]_{\rho_{N_{\mathrm{sim}}}}} R^{\mathrm{diff,sim}}_{j,j',i,i'}(\rho_{N_{\mathrm{sim}}})$$

$$\lim_{\rho\to\infty} R^{\mathrm{spec,sim}}_{j,i}(\rho) = R^{\mathrm{spec,sim}}_{j,i}(\rho_{N_{\mathrm{sim}}})$$

In praxis it is useful to generate a series of results for different values of ρ from only one actual simulation. After step 4 of the computational scheme for the wave optics simulations (compare section 2.3.1), the

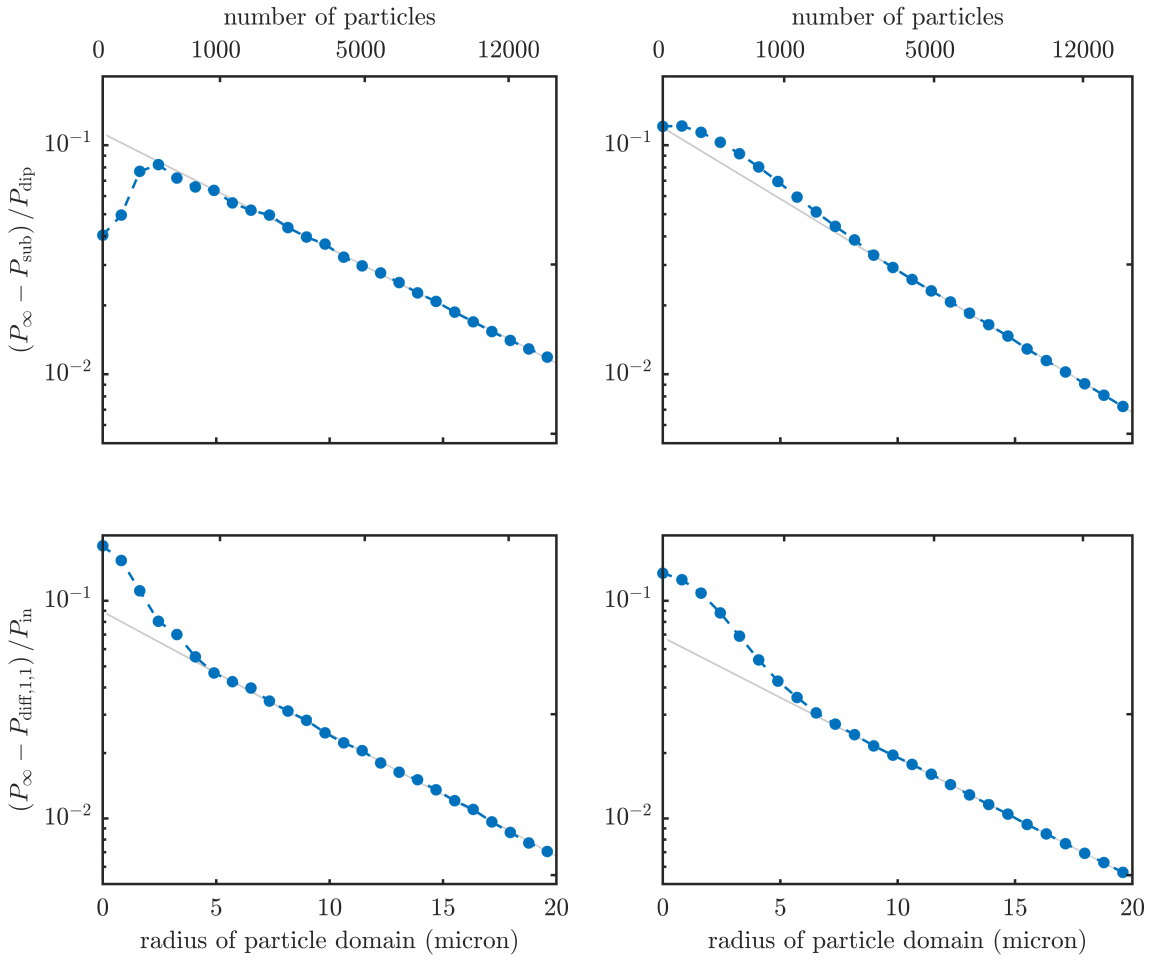

Figure 8: Convergency of the simulated power emitted/reflected into the substrate to the asymptotic value P_∞. Top row: Parallel (left) and perpendicular (right) dipole. Bottom row: TE (left) and TM (right) polarized diffuse reflection for an incoming TE polarized Gaussian wave bundle with an incident angle of 45°. The gray solid lines depict the best fit of expression (10).

solution of the scattering simulation is represented by the vector b_n^S of outgoing SVWF coefficients belonging to particle S. An approximate solution $\tilde{b}_n^S$to the smaller system of particles inside the cylinder with radius $\rho < \rho_{N_{\mathrm{sim}}}$ can be generated by using the solution for the full sample and just "switching off" all particles outside the smaller cylinder, i.e., by setting

$$\tilde{b}_n^S = \begin{cases} b_n^S & \text{for } \left|\mathbf{r}_{\parallel,S}\right|^2 \leq \rho^2 \\ 0 & \text{else} \end{cases}.$$

This way, a sweep over the particle domain radius ρ for the extrapolation to $\rho \to \infty$ can be generated very efficiently. Figure 7 displays the evolution of the power emitted/reflected into the substrate with a growing particle number for parallel and perpendicular dipole excitation, as well as for an incoming Gaussian wave bundle. For details of the simulated configuration, confer section 3. In addition to the simulation results, the solid gray curve displays expression (10) for the best-fit parameters P_∞, $\tilde{P}$ and γ. The fit was obtained by considering only the results for $\rho > 9\,\mu\mathrm{m}$ which corresponds to particle numbers $N > 3000$. The convergence of the simulation results to the asymptotic expression is displayed in figure 8. For large particle domains the exponential decay is a very good description of the simulation results, such that the approach of extrapolating the particle number by means of expression (10) is justified.

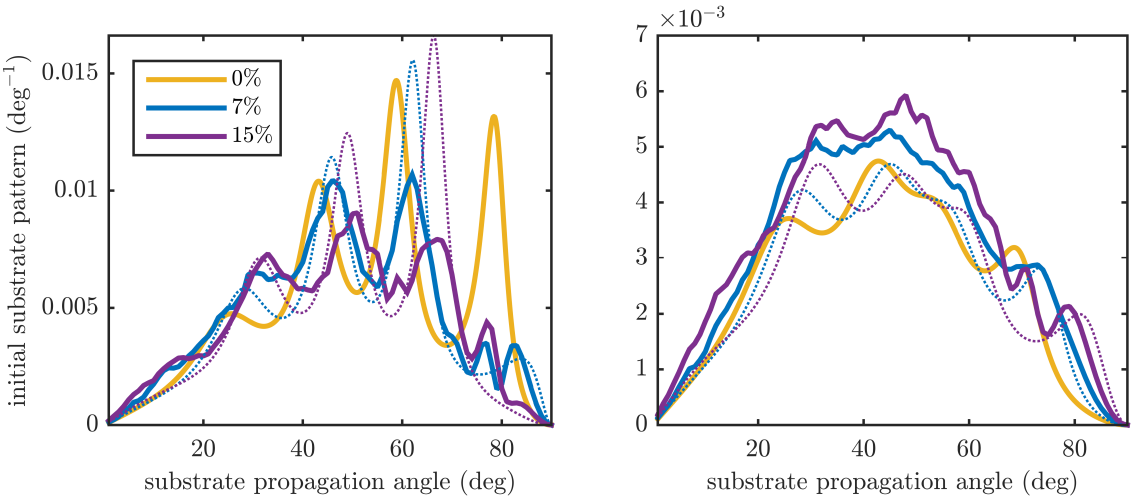

Figure 9: Initial substrate pattern $X^0_{j,i}$ for a parallel dipole, averaged over ten random realizations (solid lines), for different particle volume fractions. The dotted lines refer to an effective medium approximation of the scattering layer. The left figure shows the TE polarized emission into the substrate, and the right figure shows the TM polarized emission.

3 Results

As an exemplary application, we use the presented method to estimate the optimal particle filling fraction for a realistic OLED geometry with internal scattering particle layer. The OLED consists of the following layers: a metal electrode that is modeled as being semi infinite with a refractive index 1+6i, a 200 nm thick active organic layer with refractive index 1.75, a 100 nm thick transparent electrode with refractive index 1.85+0.01i, a 1000 nm thick scattering layer with refractive index $1.9+10^{-3}$i and finally a thick substrate layer of refractive index 1.5 that was modeled incoherently, as described above. Within the scattering layer, spherical high-index particles with radius $r = 100\,\text{nm}$ and refractive index[2] 2.5 are distributed by means of a random sequential addition algorithm. The particles are located inside a cylindrical volume with radius ρ that is adapted to yield a fixed volume filling fraction that is varied between 0 % and 20 % in the scattering layer for a given particle number. A point dipole source emitting at a fixed vacuum wavelength of $\lambda = 550\,\text{nm}$ is positioned in the middle of the active layer. The dipole moment orientation is chosen either parallel or perpendicular to the layer interfaces.

The calculations are performed by means of a self written simulation toolbox in Matlab. Equation (7) is solved with an iterative solver, namely the bi-conjugate gradient stabilized method (BiCGStab). As the particle system is too large to store the matrix $M^{SS'}_{nn'}$ in the main memory of our work station computer, matrix-vector products of type $\sum_{S',n'} M^{SS'}_{nn'} x^{S'}_{n'}$ are evaluated by calculating the matrix entries of $M^{SS'}_{nn'}$ "on the fly". A very fast scheme for the calculation of the interaction matrices W^{D} and W^{R} is thus required. We employ a lookup table approach [20] and run the most time consuming calculations on a graphics processing unit (GPU).

Figure figure 9 displays the simulated initial substrate pattern $X^0_{j,i}$ for a horizontal dipole orientation and particle filling fractions of 0 %, 7 % and 15 %. The scattering particles modify the interference pattern in the angular distribution of the initial substrate power with regard to both, the position and the amplitude of the interference maxima and minima. The diminished interference amplitude reflects the redistribution of the power over the emission angle due to the random scattering, and thereby a gradual smoothing of all angular features with increasing scattering strength. On the other hand, the shift of the interference features to larger angles can be explained by a change of the effective refractive index in

[2] Absorbing or metallic particles can be simulated with the T-matrix method, too.

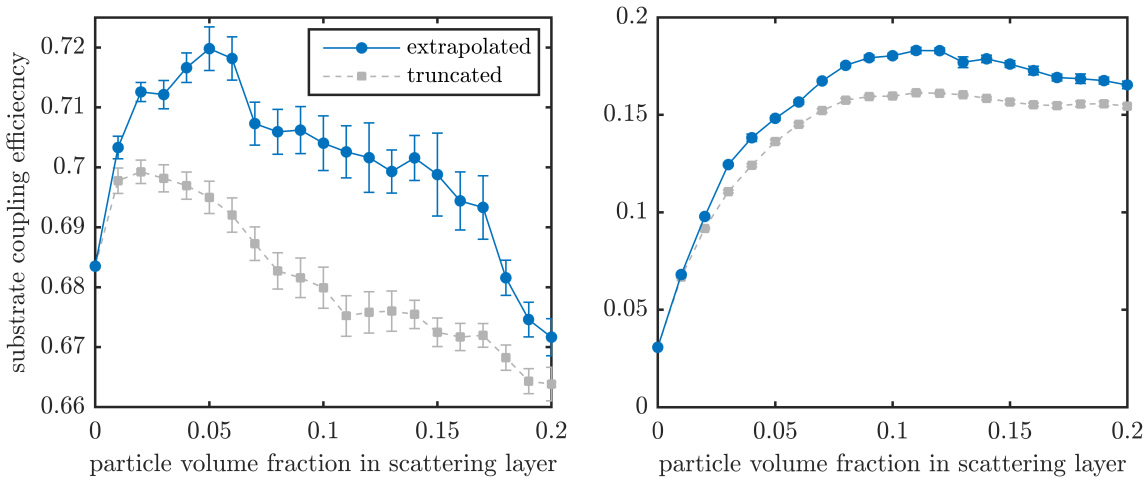

Figure 10: Substrate coupling efficiency $P^{\mathrm{sub}}/P^{\mathrm{dip}}$ for parallel (left) and perpendicular (right) dipole orientation with respect to the layer system. The errorbars indicate the statistical uncertainty of the average for 5 realizations of the random particle configuration. The blue circles represent the data extrapolated to $\rho \to \infty$ whereas the gray squares correspond to a finite number of 7500 scattering particles.

the scattering layer caused by the scattering particles. For comparison, the dotted lines show the initial substrate pattern if an effective medium approximation is used for the scattering layer. I.e., no scattering was considered, but the refractive index of the scattering layer was adjusted according to the Maxwell-Garnett formula, which leads to an increase of the effective refractive index' real part to 1.94/1.98 in the case of 7 %/15 % particle concentration. The positions of the shifted interference maxima for the effective medium approximation and for the scattering simulation are in good agreement.

Figure 10 shows the power emitted into the substrate far field, divided by the total power dissipated into the system, as a function of the particle filling fraction in the scattering layer. All simulations were truncated at $N_S = 7500$ particles, and the results were averaged over 10 random realizations of the scattering particle configurations. For parallel dipole orientation, a small but statistically significant enhancement of the substrate power coupling from 0.68 to ~ 0.72 can be attested for a filling fraction around 5 %. For perpendicular dipole orientation, the initial substrate coupling efficiency can be increased drastically from 0.03 to ~ 0.18 for particle filling fractions around 11 %. For comparison, the results for $N_S = 7500$ without extrapolation to infinite scattering samples are shown in gray.

In order to estimate the bidirectional reflectivity distribution R, simulations with an incoming Gaussian wave packet with a width of 0.03 times the vacuum wavenumber were performed. The incidence angle was varied between 0 degree and 90 degree in steps of 5 degrees. Each simulation was truncated at $N_S = 5000$ particles and the diffuse reflectivity was extrapolated to an infinite scattering layer. The simulations were not repeated for different random realizations of the scattering particle configuration. However, we have checked that the deviation for different random samples is small, as in contrast to the simulations with dipole excitation, the initial field varies rather slowly with the position in the scattering layer, such that many scattering particles are illuminated quasi homogeneously. Thereby, an effective averaging over particle configuration already takes place.

The resulting total and the diffuse reflectivity of the OLED stack with scattering layer for selected particle filling fractions are displayed in Figure 11. Again, the scattering particles lead to a shift of the interference pattern due to the modified effective refractive index of the scattering layer. An increase in the particle volume concentration from 3 % to 9 % leads to an enhanced diffuse reflectivity, but a decrease in the

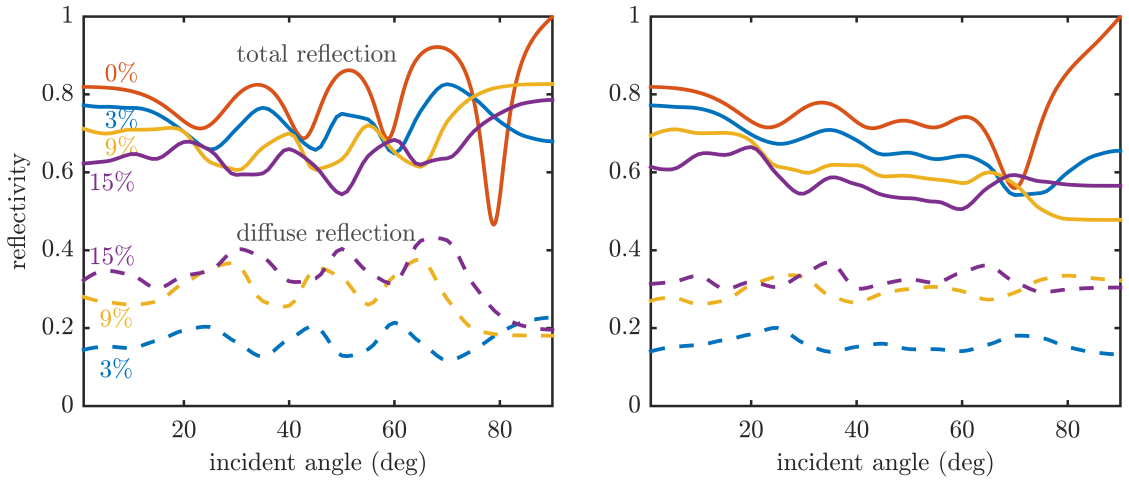

Figure 11: Simulated total (solid lines) and diffuse (dashed lines) reflectivity of the OLED thin film system including the scattering layer for TE (left) and TM (right) polarized incident wave bundles. The simulation data correspond to a particle filling fraction of 0 %, 3 %, 9 % and 15 %, respectively. The results are extrapolated to $\rho \to \infty$.

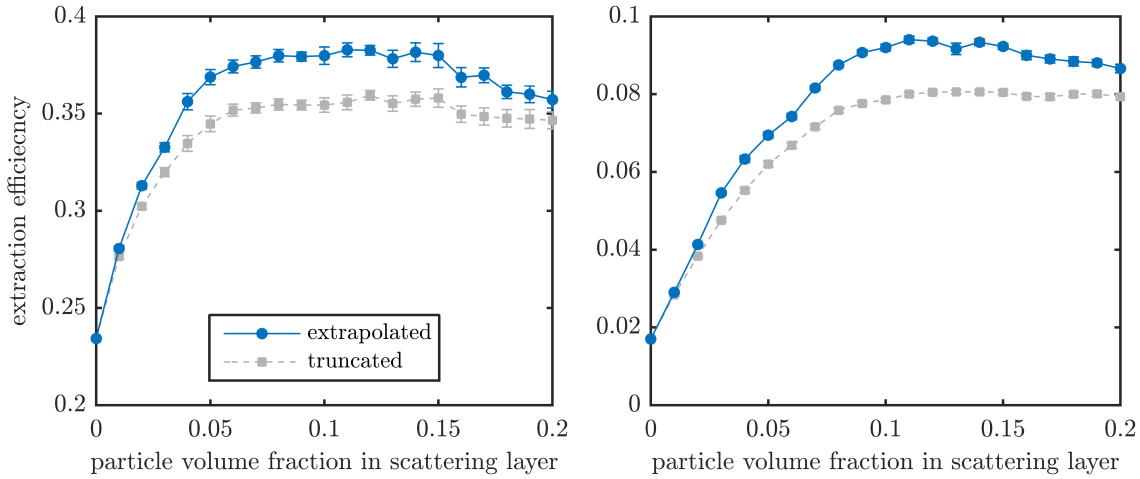

Figure 12: Extraction efficiency as a function of the particle filling fraction for parallel (left) and perpendicular (right) dipole orientation.

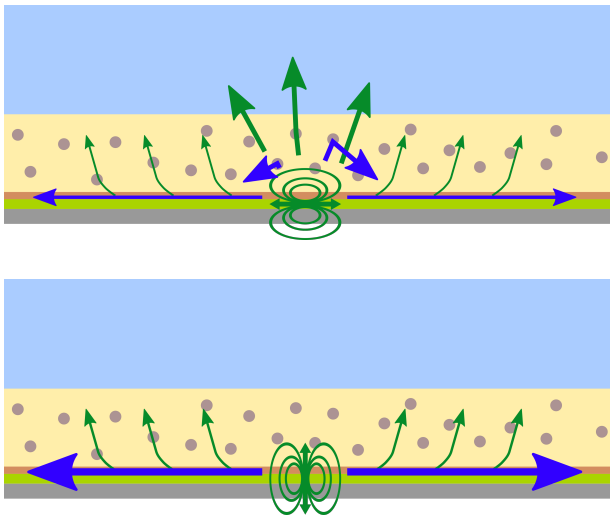

Figure 13: Coupling of radiation and waveguide modes: For parallel dipole orientation (top), the primary emission is concentrated in radiation modes, such that nearby particles cause a shadowing effect. For perpendicular dipole orientation (bottom), the primary emission is concentrated in the waveguide modes, such that all particles contribute to an enhanced outcoupling.

total reflectivity. The latter effect can be attributed to light-incoupling into waveguide modes. A further increase from 9 % to 15 % leads to a less pronounced increase in the diffuse reflectivity. Figure 12 shows the overall extraction efficiency into air. For particle filling fractions in the range of $7 - 15\,\%$ in the case of a parallel dipole orientation and $11 - 15\,\%$ in the case of a perpendicular dipole orientation, the outcoupling efficiency shows a broad maximum. In this regime, the particle concentration is high enough for a significant diffusivity in the reflection distribution, but without shadowing the direct radiation of the dipole too much. Then, an enhancement of the extraction efficiency from 0.23 for a homogeneous OLEDs without scattering particles to ~ 0.37 for parallel dipole orientation and from 0.017 to ~ 0.094 for perpendicular dipole orientation can be observed, which corresponds to an enhancement factor of 1.6 and 5.5, respectively. However, these findings are specific to the studied OLED configuration.

By comparing Figures 10 and 12, we can assess the role of internal extraction of the waveguide modes and external extraction of the substrate modes, respectively: Whereas in the case of a parallel dipole orientation, the enhancement comes predominantly from an improved extraction of the substrate modes, the extraction of the thin film bound modes is responsible for the most part of the enhancement in case of a perpendicular dipole orientation, compare also Fig. 13. The theoretical achievable enhancement of the extraction efficiency in fact depends mainly on two aspects. The first one is the efficiency of the OLED without the scattering layer as well as the distribution of the dissipated power into the various loss channels. For example, a parallel dipole orientation leads in general to a higher efficiency and a lower amount of thin film guided power than a perpendicular dipole orientation. Thus, the achievable enhancement factor and the scattering strength needed for an optimal device are lower. The second factor that influences the achievable enhancement and the optimal scattering strength is the absorption in the OLED films. If materials with high absorptivity are involved, the outcoupling needs to take place with a minimal light path length through these layers which might lead to a different optimal scattering strength compared to a configuration with highly transparent materials. An optimization of the scattering layer thus always needs to take into account the constraints imposed by the materials and device characteristics at hand.

4 Discussion and related work

The simulation method presented in section 2 relies on a very efficient scheme for the microscopic wave optics simulations as presented in section 2.3.1. However, due to the large number of required simulations to calculate a single extraction pattern, the overall numerical effort is still large. In contrast, calculations based on a ray optics treatment of the scattering layer promise a much faster evaluation of the extraction pattern. This approach was followed in [10], where the scattering layer characteristics were encoded into a bidirectional scattering distribution (BSDF). The BSDF was determined in a ray tracing algorithm, based on the differential cross sections derived from the Mie formula for the individual particles. The scattering layer is then treated as an incoherent layer in a net radiation algorithm considering the propagation through a stack of multiple coherent and incoherent layers. A good concordance between simulation and experimental results was observed [10]. The obvious question is if for the propagation through the scattering layer a ray optics treatment is justified or if wave optics calculations are necessary.

In fact, a ray optics treatment of an internal scattering layer is based on the assumption, that any coherent multiple scattering or near field interaction as well as the back-reaction of the particles' scattered field on the dipole radiative decay rate (Purcell effect) can be neglected. Ignoring these effects is probably justified if the distribution of scattering particles is dilute, the scattering layer is sufficiently thick and the layer's refractive index is matched to or higher than that of the high-index core layers of the OLED waveguide structure (typically ITO). However, for densely filled scattering layers, layers that are close to the metal electrode interface or close to the dipole emitter, clustered or unevenly distributed scattering particles or low-index scattering layers that overlap with the evanescent tail of the thin film waveguide modes (see for example [5]), a significant error from ignoring the wave-like propagation must be expected. Until now, a clear distinction of these cases, i.e., a guideline when the ray optics assumption is valid for internal scattering layers in OLEDs is lacking.

On the other hand, wave optics calculations for internal scattering layers in OLEDs have been reported in several previous papers. Here, the finite-difference time domain (FDTD) method is one popular technique [6,7,9]. One of its advantages is that the whole spectral scattering behavior of the OLED can be evaluated in only one computation. Further, it can be used to analyze the influence of a limited temporal coherence of the light source on interference effects in the light propagation through the cavity [9]. However, as the FDTD relies on a discretization of the volume that must be fine enough to correctly account for the nanoscopic geometry, the volume is limited by the growing computational burden. Typically, this issue is met by implementing reflecting or periodic boundary conditions in the lateral dimension to mimic an infinitely extended system. But care has to be taken, as not only the scattering particles, but also the dipole source is copied infinitely many times which could lead to artifacts. As an alternative, a finite-element based treatment of a single dipole source in a periodic photonic structure by means of a Floquet decomposition was presented in [26].

Another open question regarding the optimal simulation strategy refers to the averaging over the emitting dipole parameters. Even for a fixed dipole z-position and orientation (like in the here presented study), the simulated extraction pattern depends strongly on the local constellation of the emitter and the nearby scattering particles. An average can be in principle achieved through two different approaches. Either, a single dipole source is considered and the simulation is repeated several times with different random realizations of the particle locations. This is the approach followed in this paper. Alternatively, many dipole sources at different positions can be considered in the same simulation, such that an average over the local constellation of sources and scattering centers is already achieved. However, the dipoles will then interact coherently, such that repeated simulations for an average over their relative phase are necessary to achieve an incoherent sum of the dipoles [9].

Finally, the proposed simulation strategies differ in the way of representing the substrate layer. Whereas

in the here presented approach the substrate is treated as an (infinitely thick) incoherent layer, some wave optics studies represent the substrate by a coherent layer with a thickness of a few microns [7]. The advantage of this treatment is that no expensive calculation of a bidirectional reflectivity distribution is needed. However, it is an approximation to a realistic substrate layer with a thickness in the millimeter scale, and the validity of that approximation depends on the question if the figures of interest are intrigued by artificial interference effects resulting from the mesoscopic thickness of the substrate.

5 Conclusions

We have demonstrated a simulation strategy to model scattering layers in OLEDs on the basis of rigorous wave optics calculations for the light propagation in the thin film system and scattering layer, and on a ray optics treatment for the propagation in the substrate. A systematic error due to the finite size of the scattering samples was identified and a method to correct for this error was presented. The presented method allows to compute the extraction efficiency as well as the angular emission characteristics. By applying the simulation method to the optimization of the particle concentration in an internal scattering layer, we have demonstrated that this approach can be used for increasing the extraction efficiencies for a realistic OLED.

Comparing the proposed numerical strategy to other published optical simulations of internal scattering layers for light extraction from OLEDs, several possible approximations that can reduce the computational effort have been identified. These approximations include ray optics for the scattering layer, periodic boundary conditions in the lateral direction, multiple dipole sources in one wave optics simulation and the treatment of the substrate as a mesoscopic coherent layer. We hope that our method can serve as a reference for future research to clarify the validity of those approximations.

6 Acknowledgments

This work was funded by the Deutsche Forschungsgemeinschaft in the priority programme 1839. We also acknowledge support from the Karlsruhe School of Optics & Photonics (KSOP). G.G. acknowledges the support of the Helmholtz Postdoctoral Program. The authors wish to thank Horst Greiner and Lorenzo Pattelli for inspiring discussions.

References

[1] M. Gather and S. Reineke, "Recent advances in light outcoupling from white organic light-emitting diodes," *Journal of Photonics for Energy*, vol. 5, p. 057607, 2015.

[2] G. Gomard, J. B. Preinfalk, A. Egel, and U. Lemmer, "Photon management in solution-processed organic light-emitting diodes: a review of light outcoupling micro- and nanostructures," *J. Photonics Energy*, vol. 6, no. 3, p. 030901, 2016.

[3] H. Bechtel, W. Busselt, and J. Opitz, "Subwavelength particle layers for improved light outcoupling of OLEDs," *SPIE Proceedings*, vol. 5519, 2004.

[4] N. Nakamura, N. Fukumoto, F. Sinapi, N. Wada, Y. Aoki, and K. Maeda, "40 . 4 : Glass Substrates for OLED Lighting with High Out-coupling Efficiency OLED on a Glass Scattering Layer," in *SID Symposium Digest of Technical Papers*. Blackwell Publishing Ltd, 2009, pp. 603–606.

[5] H.-W. Chang, J. Lee, S. Hofmann, Y. Hyun Kim, L. Müller-Meskamp, B. Lüssem, C.-C. Wu, K. Leo, and M. C. Gather, "Nano-particle based scattering layers for optical efficiency enhancement of organic light-emitting diodes and organic solar cells," *Journal of Applied Physics*, vol. 113, no. 20, p. 204502, 2013.

[6] J. Lee, Y. Y. Kwon, E.-H. Choi, J. Park, H. Yoon, and H. Kim, "Enhancement of light-extraction efficiency of organic light-emitting diodes using silica nanoparticles embedded in TiO2 matrices," *Opt. Express*, vol. 22, no. S3, pp. A705–A714, 2014.

[7] M.-C. Oh, J.-H. Park, H. J. Jeon, and J. S. Go, "Hollow-core polymeric nanoparticles for the enhancement of OLED outcoupling efficiency," *Displays*, 2014.

[8] D. Riedel, T. Wehlus, T. C. Reusch, and C. J. Brabec, "Polymer-based scattering layers for internal light extraction from organic light emitting diodes," *Organic Electronics*, vol. 32, pp. 27–33, 2016.

[9] J.-W. Kim, J.-H. Jang, M.-C. Oh, J.-W. Shin, D.-H. Cho, J.-H. Moon, and J.-I. Lee, "FDTD analysis of the light extraction efficiency of OLEDs with a random scattering layer," *Opt. Express*, vol. 22, no. 1, pp. 498–507, 2014.

[10] S. Altazin, C. Reynaud, U. M. Mayer, T. Lanz, K. Lapagna, R. Knaack, L. Penninck, C. Kirsch, K. P. Pernstich, S. Harkema, D. Hermes, and B. Ruhstaller, "38.3: Simulations, Measurements, and Optimization of OLEDs with Scattering Layer," *SID Symposium Digest of Technical Papers*, vol. 46, no. 1, pp. 564–567, 2015.

[11] A. Egel and U. Lemmer, "Dipole emission in stratified media with multiple spherical scatterers: Enhanced outcoupling from OLEDs," *Journal of Quantitative Spectroscopy and Radiative Transfer*, vol. 148, pp. 165–176, 2014.

[12] R. Chance, A. Prock, and R. Silbey, "Molecular fluorescence and energy transfer near interfaces," *Adv. Chem. Phys*, 1978.

[13] A. Sommerfeld, "Über die Ausbreitung der Wellen in der drahtlosen Telegraphie," *Annalen der Physik*, 1909.

[14] G. Kristensson, "Electromagnetic scattering from buried inhomogeneities - a general three-dimensional formalism," *Journal of Applied Physics*, vol. 51, no. 7, p. 3486, 1980.

[15] A. Bostrom, G. Kristensson, and S. Strom, "Transformation Properties of Plane, Spherical and Cylindrical Scalar and Vector Wave Functions," in *Field Representations and Introduction to Scattering*, 1991, pp. 165–210.

[16] G. Videen, "Light scattering from a sphere on or near a surface," *Journal of the Optical Society of America A*, vol. 8, no. 3, p. 483, 1991.

[17] T. Wriedt and A. Doicu, "Light scattering from a particle on or near a surface," *Optics Communications*, vol. 152, no. 4-6, pp. 376–384, 1998.

[18] D. W. Mackowski, "Exact solution for the scattering and absorption properties of sphere clusters on a plane surface," *Journal of Quantitative Spectroscopy and Radiative Transfer*, vol. 109, no. 5, pp. 770–788, 2008.

[19] A. Egel, D. Theobald, Y. Donie, U. Lemmer, and G. Gomard, "Light scattering by oblate particles near planar interfaces: on the validity of the T-matrix approach," *Opt. Express*, vol. 24, no. 22, p. 25154, 2016.

[20] A. Egel, S. W. Kettlitz, and U. Lemmer, "Efficient evaluation of Sommerfeld integrals for the optical simulation of many scattering particles in planarly layered media," *Journal of the Optical Society of America A*, vol. 33, no. 4, p. 698, 2016.

[21] P. C. Waterman, "Matrix formulation of electromagnetic scattering," *Proceedings of the IEEE*, vol. 53, no. 8, pp. 805–812, 1965.

[22] M. I. Mishchenko, G. Videen, V. A. Babenko, N. G. Khlebtsov, and T. Wriedt, "T-matrix theory of electromagnetic scattering by partciles and its applications: a comprehensive reference database," *Journal of Quantitative Spectroscopy and Radiative Transfer*, vol. 88, no. 1-3, pp. 357–406, 2004.

[23] Y. A. Doicu, A; Wriedt, T; Eremin, *Light Scattering by Systems of Particles*, 1st ed. Berlin, Heidelberg: Springer-Verlag, 2006.

[24] L. Novotny, *Principles of Nano-Optics*. Cambridge: Cambridge University Press, 2006, vol. 1, no. 4.

[25] C. Wiesmann, "Nano-structured LEDs - Light extraction mechanisms and applications," PhD Thesis, University of Regensburg, 2010.

[26] L. Zschiedrich and H. Greiner, "Numerical analysis of nanostructures for enhanced light extraction from OLEDs," *SPIE Proceedings*, 2013.